Modelling the spread of serotype-2 vaccine derived-poliovirus outbreak in Pakistan and Afghanistan to inform outbreak control strategies in the context of the COVID-19 pandemic

(Supplementary Information)

Natalia A Molodecky, Hamid Jafari, Rana M Safdar, Jamal A Ahmed, Abdirahman Mahamud, Ananda S Bandyopadhyay, Hemant Shukla, Arshad Quddus, Michel Zaffran, Roland W Sutter, Nicholas C Grassly and Isobel M Blake

Table of Contents

1 Methods

1.1 Geodata

National, provincial and district boundaries for Pakistan and Afghanistan were obtained from the World Health Organization (WHO). The district-level administrative boundaries in Pakistan have changed over time. In order to explore incidence over time, we retain the boundaries of districts in 2010 for the entire time series. Additionally, we consider Karachi as one administrative unit. The geographic size of provinces in Afghanistan are similar to districts in Pakistan and therefore, provinces were used as the geographic scale in Afghanistan (Figure S1). A total of 139 districts of Pakistan and 34 provinces of Afghanistan were included in the model. All geographic units are hereafter referred to as districts.

Figure S1: Map of Pakistan and Afghanistan, with the first-level administrative boundaries.

Note: The publication of these maps does not imply the expression of any opinion whatsoever on the part of WHO concerning the legal status of any territory, city, or area or of its authorities, or concerning the delimitation of its frontiers or boundaries.

1.2 Underlying cVDPV2 transmission model

A schematic of the states and state transitions for the VDPV2 transmission model is provided in Figure S2. The model state and input parameter names and values are presented in Table S1 and Table S2, respectively.

Table S1: cVDPV2 transmission model schematic state and parameter names

Parameters	Description
λ	Force of infection
κ	Reversion probability
γ	Recovery rate
τ	Reporting rate
μ	Birth and death rate
ν	Latency period
ψ	Waning rate
ω	Susceptibility scaling factor for those with waned mucosal immunity
ξ	Scaling factor for Sabin2 R_0
σ	Boolean parameter for time of campaign
c	Vaccination campaign coverage
z	Rate of vaccination with three OPV2 doses through RI
y	Rate of vaccination with one IPV dose through RI
e	Vaccine efficacy
States	**Description**
S	Suscptible
E	Exposed
I	Infected with the original VDPV2
J	Infected with newly reverted Sabin2 to VDPV2
O	Infected with Sabin2
R	Recovered
W	Waned mucosal immunity
V	Immunized with IPV

Figure S2: State transitions for VDPV2 transmission model between 2010-2016. Blue lines indicate movement between states at a constant rate and red lines indicate movement between states resulting from an SIA campaign with tOPV. Per-capita rates are in blue and state transitions are in black.

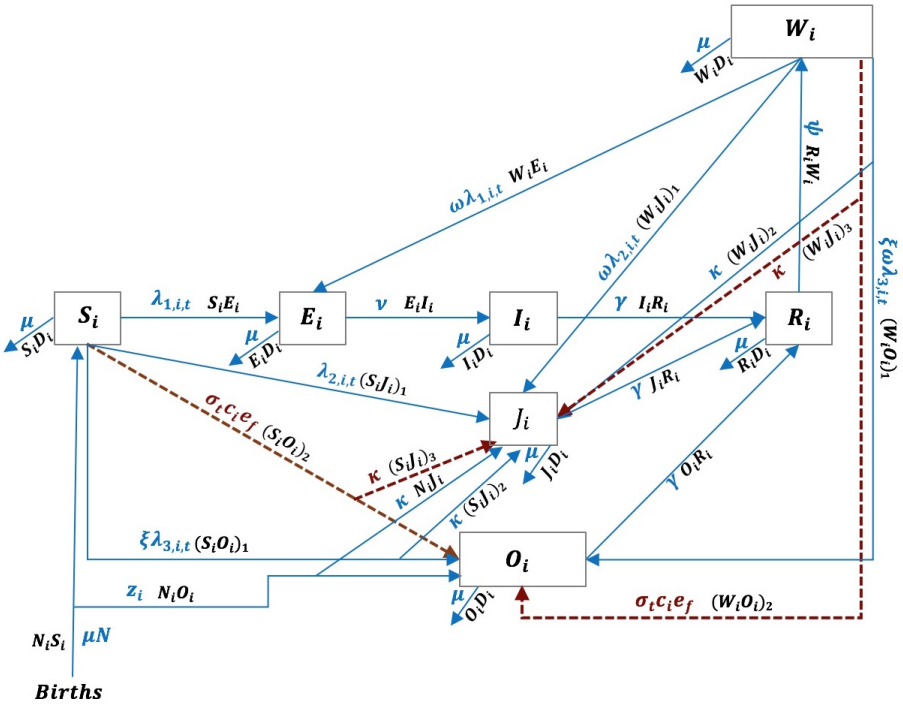

Figure S3: State transitions for VDPV2 transmission model for forward simulations, including immunization with IPV following OPV2 withdrawal (i.e. post April 2016). Blue lines indicate movement between states at a constant rate, red lines indicate movement between states resulting from an SIA with mOPV2 and orange lines indicated immunization with IPV, either in RI or SIAs. Per-capita rates are in blue and state transitions are in black. New adaptations to model are in bold.

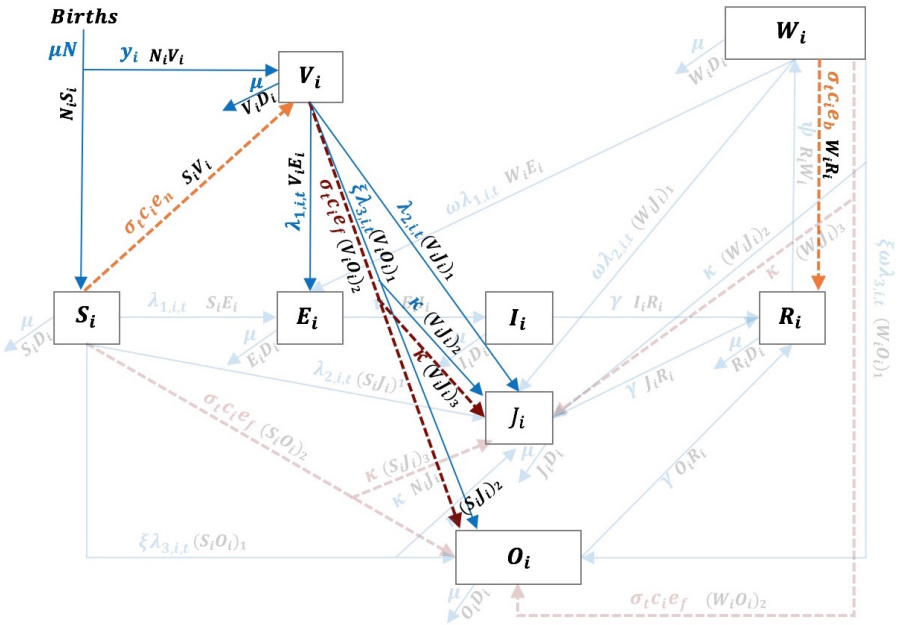

Due to the fact that there are multiple ways of transitioning between some compartments, we

have denoted these transitions with subscripts 1, 2 and 3. Subscript 1 indicates direct transition between compartments, whereas subscripts 2 and 3 indicate indirect transition between compartments (i.e. those that include an intermediate step). Subscript 2 corresponds to a constant rate at each time step t and subscript 3 corresponds to time t of each SIA. For example, $(S_iJ_i)_1$, $(S_iJ_i)_2$ and $(S_iJ_i)_3$ correspond to three different ways of transitioning between S and J; specifically, through transmission of VDPV2, reversion after secondary spread of Sabin-2 vaccine virus and reversion after SIA vaccination, respectively.

Table S2: Parameter estimates for the cVDPV2 transmission model.

Parameters	Estimates (95% CIs)	Source
Recovery rate, γ	1/14	Evidence from[1][1]
Reporting rate, τ	1/400	Evidence from [2, 3]
Birth and death rate, μ	1/1581 per day	Median time in cohort (3 years)
Latency period, ν	4 days	Evidence from [4]
Number of initial cVDPV2 infections	400	Reporting rate
Sabin R_0	0.9	Evidence from [5, 6][2]
Secondary spread of OPV2	42%	Seroprevalence of serotype-2 in non-immunized populations [7]
Waning rate, ψ	1/527 per day	Evidence from[8]
Susceptibility scaling factor for those with waned mucosal immunity, ω	0.5	Evidence from[8]
Efficacy of tOPV (serotype-2)	0.48	Evidence from [9]
Efficacy of mOPV2	0.68	Evidence from [10, 11, 12, 13, 14][3]
Efficacy of IPV (naive)	0.6	Evidence from [15]
Efficacy of IPV (boost)	0.9	Evidence from [15]

[1] Duration of infectiousness based on this study was extended given the greater contribution of fecal-oral transmission in this population (which has longer shedding of virus compared to oral-oral transmission [16]). [2] Support for R_0 of Sabin-2 vaccine virus <1 is based evidence following OPV2 withdrawal (i.e. rapid decline if Sabin-2 in environment and AFP cases). [3] Following a review of seroconversion following OPV across multiple geographies adjusting for vaccine time and <5 year old mortality (proxy for development) and assuming an all or nothing response of OPV. See details in Section 1.2.5.

1.2.1 Force of infections

There are three distinct force of infections $\lambda_{i,t+1}$ for the VDPV2 model, defined as $\lambda_{1,i,t+1}$, $\lambda_{2,i,t+1}$, $\lambda_{3,i,t+1}$. The force of infection $\lambda_{1i,t+1}$ for a susceptible in each district i is a function of time t and becoming infected with VDPV2, and is defined by manuscript equation (1). The force of infection $\lambda_{2,i,t+1}$ is the same as manuscript equation (1) but $I_{i,t}$ and $I_{j,t}$ are replaced by $J_{i,t}$ and $J_{j,t}$ (the number of children infected with reverted Sabin-2 vaccine virus to VDPV2) and for $\lambda_{3,i,t+1}$ $I_{i,t}$ and $I_{j,t}$, substituted for $O_{i,t}$ and $O_{j,t}$ (the number of children infected with Sabin-2 vaccine virus (i.e. OPV)).

The force of infection for transmission of Sabin-2 ($\lambda_{3,i,t+1}$) was scaled by a factor ξ that results in

the Sabin R_0 (from the dominant eigenvalue of the next generation matrix) to be <1. In the model, we assumed a Sabin R_0 value of 0.9. There is consistent support that the R_0 of Sabin vaccine virus is <1, as the spread of Sabin-2 does not persist and subsequently immunize entire populations, as evidenced by the rapid decline of Sabin-2 in the environment and AFP cases following OPV withdrawal (resulting from mass tOPV immunization immediately prior to OPV2 withdrawal) [6, 5].

1.2.2 Seasonality

We extended this model to allow the transmission rate to be seasonal. Key features of seasonality are amplitude and phase, where A is the amplitude of seasonal variation in transmission (i.e. strength of seasonal forcing) and ϕ is the horizontal phase shift. Each transmission coefficient in the model was modified to account for seasonal transmission in the following way:

$$\beta_{s,x,t} = \beta_x(1 + A\cos(2\pi(t/365) - \phi)) \tag{1}$$

where $\beta_{s,x,t}$ is the seasonal transmission coefficient at time t, with distinct estimates for each time point in a 1 year period; with x corresponding to either local l or between-district b transmission. The phase, ϕ, was assumed to be 16 July and was based on [17] and preliminary genetic analysis of WPV1 sequences reported from Pakistan using methods described in [18].

In order to estimate A, we developed a similar state space stochastic mathematical model as described above but fitted it to historic daily incidence of WPV1 for 2010-2016. The large number of WPV1 cases over time (in contrast to cVDPV2s), provided more information on the seasonal dynamics of transmission (summary of methods and results provided in Supplementary Appendix I, Section 3). The estimated A from this model was retained for the 2010-2016 cVDPV2 model validation.

For the model calibration in 2019-2020, fitting the model using the same amplitude resulted in a poor correspondence between model simulations and observed cases. A better fit was achieved through scaling the amplitude by the same factor that the R_0 was reduced by in the model calibration for this period. A comparison of log likelihood values for each amplitude is given in Table S3.

1.2.3 Waning of mucosal immunity

Children in the recovered R state were assumed to have complete mucosal immunity and therefore could not be infected or contribute to transmission. Mucosal immunity was assumed to last for a median duration of 1 year, after which children entered the waned, W, compartment. Therefore, the waning rate ψ was 1/527 per day. This was based on evidence from India suggesting significant waning within 1 year of vaccination [8]. Children in the waning state were assumed to be half as susceptible as individuals infected for the first time and although could be reinfected they could not develop disease. Previous evidence suggests that significant mucosal protection remains in those previously

well-immunized but with waned mucosal immunity (odds ratio of shedding serotype-2 vaccine virus after challenge in children with waned mucosal immunity (i.e. ≥6 months since last tOPV dose) compared to poorly vaccinated children was 0.53 (95% CI, 0.25–1.13) [8].

The force of VDPV2 infection per individual with waned mucosal immunity was defined as $\omega\lambda_{x,i,t}$, where x corresponds to 1, 2 or 3. The factor ω scales the force of infection λ by a factor to capture the reduced susceptibility in those with waned mucosal immunity (we assumed ω=0.5).

1.2.4 Duration of Sabin (OPV) or VDPV2 infection

The rate of recovery for children infected with either Sabin-2 or reverted Sabin-2 virus was assumed to be the same as that with VDPV2. The number of children transitioning from O_i and J_i to R_i is therefore determined by the rate of recovery, γ.

1.2.5 Vaccination

For RI prior to April 2016, a child could be expected to receive up to three trivalent OPV (tOPV) doses, captured in the model by moving a proportion of susceptible children, z_i, to the R_i compartment from birth, whereby $z_i = k_i[e_t(1+(1-e_t)+(1-e_t)^2]$ and k_i is the district specific coverage of receiving three tOPV doses through RI and e_t is the per dose efficacy of tOPV against serotype-2 (i.e. 0.48 [9]). Following OPV2 withdrawal, tOPV was stopped in RI and one dose of IPV was introduced. Vaccination with one dose of IPV through RI was incorporated into the model as a rate of movement from births directly into the V_i compartment. The proportion of births y_i immunised with IPV was based on the RI coverage, k_i, and vaccine efficacy of one dose of IPV in OPV-naive children, e_n (i.e. 0.60 [15]): $y_i = k_i e_n$. Importantly we assume immunisation of susceptible children with IPV protects against poliomyelitis but does not prevent infection with poliovirus.

Additionally, susceptible children or children with waned mucosal immunity could be immunised through SIAs at specific points in time (that we index by the boolean parameter, σ_t, that equals 1 at times of vaccination campaigns and zero when no vaccination campaigns occur). The probability of a child becoming immunised through an SIA is $\sigma_t c_i e_f$, where c_i is the district-specific SIA coverage and e_f is the per dose efficacy of the vaccine used against serotype-2 (i.e. tOPV or mOPV2, prior to and following 2016, respectively). While the efficacy of mOPV2 has not been conclusively determined, we assumed the per dose efficacy of mOPV2 to be 68%. After compiling data on seroconversion following tOPV or mOPV2 administration [10, 11, 12, 13, 14] we measured the association between seroconversion and vaccine type and <5 year old mortality (as a proxy for development) using binomial regression. Seroconversion was lower following administration of tOPV compared to mOPV2 (OR 0.25, 95%CI 0.11,0.48) and populations with low <5 year old mortality (<25 births per 1000 live births) were more likely to seroconvert (OR 4.6, 95%CI 2.5 – 9.4) compared to those with high child mortality (75 deaths per 100 live births). Assuming an all or nothing response, we converted the probability

of seroconverting to per dose efficacies, accounting for the number of OPV doses received prior to seroconversion. Pakistan has a high child mortality rate and we estimated mOPV2 efficacy to be 0.68 and tOPV efficacy to be 0.50.

On successful immunisation with tOPV or mOPV2, most children (1-κ) enter the Sabin-2 vaccinated state O_i for a mean of 14 days after which they progress to full mucosal immunity (R_i). However, we assume Sabin-2 virus will instantaneously revert to create a new circulating VDPV2 in a small proportion of immunised children (κ) and these children enter state J_i (whereby J_i is equally as infectious as I_i).

Vaccination with IPV in SIAs was incorporated into the model by moving a proportion of susceptible children into the IPV V_i state and waned children W_i into the recovered state R_i at the time of each SIA (i.e. seroconversion of naive children or boosting of mucosal immunity in previously OPV-immunized children, respectively). The probability of transitioning from S_i to V_i and W_i to R_i is a product of the vaccination campaign coverage and the vaccine efficacy: $\sigma_t c_i e_x$, where x corresponds to either n (naive) or b (boost). The vaccine efficacy of IPV applied to children in S state assumes no prior exposure to OPV2 (i.e. OPV2 naive with efficacy e_n of 0.6) and that applied to the W state assumes previous OPV2 exposure (i.e. boosting of mucosal immunity with efficacy e_b of 0.9 [15].

Vaccination of IPV-immunised recipients with mOPV2 in SIAs was incorporated by moving a proportion $(\sigma_t c_i e_x)$(1-κ) of children from the V_i state into the O_i state. A small proportion of those transitioning out of V_i state moved into the J_i state at the time of each SIA, $(\sigma_t c_i e_x)(\kappa)$. Here we assume that OPV induces mucosal immunity in previously IPV immunized individuals and that prior exposure to IPV (in OPV2-naive individuals) does not reduce OPV take or reduce the risk of reversion, as evidenced by the lack of protection of IPV against vaccine-associated paralytic poliomyelitis

1.2.6 Movement between states and state transitions for 2010-2016

The number of children moving between states at time t is determined by drawing random numbers from the multinomial distributions based on the probability defined by the transition rates or probabilities multiplied by dt (a small time step of 0.25 days). In the case of vaccination and reversion, the number of children vaccinated and number with reverted Sabin-2 infection is drawn from the binomial distribution. The movement between states are as follows:

$$(Z_t^{S_iE_i}, Z_t^{(S_iJ_i)_1}, Z_t^{(S_iO_i)_1}, Z_t^{S_iD_i}) \sim \text{Multinomial}(S_{i,t-1}, \boldsymbol{\rho}_{i,S})$$
$$\boldsymbol{\rho}_{i,S} = (\lambda_{1,i,t}dt, \lambda_{2,i,t}dt, \xi\lambda_{3,i,t}dt, \mu dt)$$

$$Z_t^{(S_iJ_i)_2} \sim \text{Binomial}(Z_t^{(S_iO_i)_1}, \kappa)$$

$$(Z_t^{E_iI_i}, Z_t^{E_iD_i}) \sim \text{Multinomial}(E_{i,t-1}, \boldsymbol{\rho}_{i,E})$$
$$\boldsymbol{\rho}_{i,E} = (\nu dt, \mu dt)$$

$$(Z_t^{I_iR_i}, Z_t^{I_iD_i}) \sim \text{Multinomial}(I_{i,t-1}, \boldsymbol{\rho}_{i,I})$$
$$\boldsymbol{\rho}_{i,I} = (\gamma dt, \mu dt)$$

$$(Z_t^{R_iW_i}, Z_t^{R_iD_i}) \sim \text{Multinomial}(R_{i,t-1}, \boldsymbol{\rho}_{i,R})$$
$$\boldsymbol{\rho}_{i,R} = (\psi dt, \mu dt)$$

$$(Z_t^{J_iR_i}, Z_t^{J_iD_i}) \sim \text{Multinomial}(J_{i,t-1}, \boldsymbol{\rho}_{i,J})$$
$$\boldsymbol{\rho}_{i,J} = (\gamma dt, \mu dt)$$

$$(Z_t^{O_iR_i}, Z_t^{O_iD_i}) \sim \text{Multinomial}(O_{i,t-1}, \boldsymbol{\rho}_{i,O})$$
$$\boldsymbol{\rho}_{i,O} = (\gamma dt, \mu dt)$$

$$(Z_t^{W_iE_i}, Z_t^{(W_iJ_i)_1}, Z_t^{(W_iO_i)_1}, Z_t^{W_iD_i}) \sim \text{Multinomial}(W_{i,t-1}, \boldsymbol{\rho}_{i,W})$$
$$\boldsymbol{\rho}_{i,W} = (\omega\lambda_{1,i,t}dt, \omega\lambda_{2,i,t}dt, \omega\xi\lambda_{3,i,t}dt, \mu dt)$$

$$Z_t^{(W_iJ_i)_2} \sim \text{Binomial}(Z_t^{(W_iO_i)_1}, \kappa)$$

$$Z_t^{(S_iO_i)_2} \sim \text{Binomial}(S_{i,t-1}, \sigma_t c_{i,t} e_f)$$
$$Z_t^{(S_iJ_i)_3} \sim \text{Binomial}(Z_t^{(S_iO_i)_2}, \kappa)$$

$$Z_t^{(W_iO_i)_2} \sim \text{Binomial}(W_{i,t-1}, \sigma_t c_{i,t} e_f)$$
$$Z_t^{(W_iJ_i)_3} \sim \text{Binomial}(Z_t^{(W_iO_i)_2}, \kappa)$$

$$Z_t^{N_iS_i} \sim \text{Binomial}(N_{i,t-1}, \mu dt)$$
$$Z_t^{N_iO_i} \sim \text{Binomial}(Z_t^{N_iS_i}, z_i dt)$$

$$Z_t^{N_iJ_i} \sim \text{Binomial}(Z_t^{N_iO_i}, \kappa)$$

The state transitions for the VDPV2 transmission model at time t are as follows:

$$S_{i,t} = S_{i,t-1} - Z_t^{S_iE_i} - Z_t^{(S_iJ_i)_1} - Z_t^{(S_iO_i)_1} - Z_t^{S_iD_i} + Z_t^{N_iS_i} - Z_t^{N_iO_i} - Z_t^{(S_iO_i)_2}$$

$$E_{i,t} = E_{i,t-1} + Z_t^{S_iE_i} - Z_t^{E_iI_i} - Z_t^{E_iD_i} + Z_t^{W_iE_i}$$

$$I_{i,t} = I_{i,t-1} + Z_t^{E_iI_i} - Z_t^{I_iR_i} - Z_t^{I_iD_i}$$

$$R_{i,t} = R_{i,t-1} - Z_t^{R_iW_i} - Z_t^{R_iD_i} + Z_t^{I_iR_i} + Z_t^{J_iR_i} + Z_t^{O_iR_i}$$

$$J_{i,t} = J_{i,t-1} - Z_t^{J_iR_i} - Z_t^{J_iD_i} + Z_t^{(S_iJ_i)_1} + Z_t^{(W_iJ_i)_1} + Z_t^{(S_iJ_i)_2} + Z_t^{(W_iJ_i)_2} + Z_t^{(S_iJ_i)_3} + Z_t^{(W_iJ_i)_3} + Z_t^{N_iJ_i}$$

$$O_{i,t} = O_{i,t-1} - Z_t^{O_iR_i} - Z_t^{O_iD_i} + Z_t^{(S_iO_i)_1} - Z_t^{(S_iJ_i)_2} + Z_t^{(S_iO_i)_2} - Z_t^{(S_iJ_i)_3} + Z_t^{N_iO_i} -$$
$$Z_t^{N_iJ_i} + Z_t^{(W_iO_i)_1} - Z_t^{(W_iJ_i)_2} + Z_t^{(W_iO_i)_2} - Z_t^{(W_iJ_i)_3}$$

$$W_{i,t} = W_{i,t-1} - Z_t^{W_iE_i} - Z_t^{(W_iJ_i)_1} - Z_t^{(W_iO_i)_1} - Z_t^{W_iD_i} + Z_t^{R_iW_i} - Z_t^{(W_iO_i)_2}$$

1.2.7 Movement between states and state transitions for post OPV2 withdrawal, from April 2016

The number of children moving from the V state at time t is determined by drawing random numbers from the multinomial distribution based on the probability defined by the transition rates or probabilities. In children vaccinated with IPV in RI, the force of VDPV2 infection is assumed to be the same as for fully susceptible children (but risk of paralysis is zero). Therefore, the movement from V is defined by:

$$(Z_t^{V_iE_i}, Z_t^{(V_iJ_i)_1}, Z_t^{(V_iO_i)_1}, Z_t^{V_iD_i}) \sim \text{Multinomial}(V_{i,t-1}, \boldsymbol{\rho}_{i,V})$$
$$\boldsymbol{\rho}_{i,V} = (\lambda_{1,i,t}dt, \lambda_{2,i,t}dt, \xi\lambda_{3,i,t}dt, \mu dt)$$

$$Z_t^{(V_iJ_i)_2} \sim \text{Binomial}(Z_t^{(V_iO_i)_1}, \kappa)$$

$$Z_t^{N_iS_i} \sim \text{Binomial}(N_{i,t-1}, \mu dt)$$
$$Z_t^{N_iV_i} \sim \text{Binomial}(Z_t^{N_iS_i}, y_i dt)$$

$$Z_t^{S_iV_i} \sim \text{Binomial}(S_{i,t-1}, \sigma_t c_i e_n)$$
$$Z_t^{W_iR_i} \sim \text{Binomial}(W_{i,t-1}, \sigma_t c_i e_b)$$

$$Z_t^{(V_iO_i)_2} \sim \text{Binomial}(V_{i,t-1}, \sigma_t c_i e_f)$$
$$Z_t^{(V_iJ_i)_3} \sim \text{Binomial}(Z_t^{(V_iO_i)_2}, \kappa)$$

The state transitions for the VDPV2 simulation model post-OPV2 withdrawal are as follows:

$$S_{i,t} = S_{i,t-1} - Z_t^{S_iE_i} - Z_t^{S_iD_i} - Z_t^{(S_iJ_i)_1} - Z_t^{(S_iO_i)_1} - Z_t^{(S_iO_i)_2} - Z_t^{S_iV_i} + Z_t^{N_iS_i} - Z_t^{N_iV_i}$$

$$E_{i,t} = E_{i,t-1} + Z_t^{S_iE_i} - Z_t^{E_iI_i} - Z_t^{E_iD_i} + Z_t^{W_iE_i} + Z_t^{V_iE_i}$$

$$I_{i,t} = I_{i,t-1} + Z_t^{E_iI_i} - Z_t^{I_iR_i} - Z_t^{I_iD_i}$$

$$R_{i,t} = R_{i,t-1} - Z_t^{R_iW_i} - Z_t^{R_iD_i} + Z_t^{I_iR_i} + Z_t^{J_iR_i} + Z_t^{O_iR_i} + Z_t^{W_iR_i}$$

$$V_{i,t} = V_{i,t-1} - Z_t^{V_iE_i} - Z_t^{(V_iJ_i)_1} - Z_t^{(V_iO_i)_1} - Z_t^{V_iD_i} + Z_t^{S_iV_i} + Z_t^{N_iV_i} - Z_t^{(V_iO_i)_2}$$

$$J_{i,t} = J_{i,t-1} - Z_t^{J_iR_i} - Z_t^{J_iD_i} + Z_t^{(S_iJ_i)_1} + Z_t^{(S_iJ_i)_2} + Z_t^{(S_iJ_i)_3} + Z_t^{(W_iJ_i)_1} + Z_t^{(W_iJ_i)_2} - Z_t^{(W_iJ_i)_3} + Z_t^{(V_iJ_i)_1} - Z_t^{(V_iJ_i)_2} + Z_t^{(V_iJ_i)_3}$$

$$O_{i,t} = O_{i,t-1} - Z_t^{O_iR_i} - Z_t^{O_iD_i} + Z_t^{(S_iO_i)_1} - Z_t^{(S_iJ_i)_2} + Z_t^{(S_iO_i)_2} - Z_t^{(S_iJ_i)_3} + Z_t^{(W_iO_i)_1} - Z_t^{(W_iJ_i)_2} + Z_t^{(W_iO_i)_2} -$$
$$Z_t^{(W_iJ_i)_3} + Z_t^{(V_iO_i)_1} - Z_t^{(V_iJ_i)_2} + Z_t^{(V_iO_i)_2} - Z_t^{(V_iJ_i)_3}$$

$$W_{i,t} = W_{i,t-1} - Z_t^{W_iE_i} - Z_t^{(W_iJ_i)_1} - Z_t^{(W_iO_i)_1} - Z_t^{W_iD_i} + Z_t^{R_iW_i} - Z_t^{W_iR_i} - Z_t^{(W_iO_i)_2}$$

1.2.8 Observation model

The probability of an infected child being reported as a cVDPV2 case C is assumed to follow a binomial distribution and is defined by the reporting rate τ (i.e. 1:400):

$$C_{i,t} \sim \text{Binomial}(H_{i,t}, \tau_t)$$

where $H_{i,t}$ is the number of children who complete the incubation period and develop poliomyelitis in district i at time t. The incubation period was assumed to be 16.5 days and was based on fitting independent data from 36 cases of paralytic poliomyelitis with known dates of exposure to an infected individual using a lognormal distribution [19, 20, 4]. In order to have an incubation period that followed the Markov property (i.e. each compartment having its own exponential distribution), an Erlang distribution was fitted to these data. The Erlang distribution had shape of 6 compartments and rate of transitioning between compartments of 0.329 days^{-1}.

1.2.9 Defining the process model

We used the R package POMP [21], which enables simulating and fitting partially-observed Markov process models (i.e. state-space models) to time series. POMP assumes that the state at time $t+1$ depends only on the state at time t and on some parameters (θ). The true underlying state process is defined by: $X_{t+1} \sim f(X_t, \theta)$ and the measurement or observation process are linked to the state process in the following way: $Y_t \sim f(X_t, \tau)$. The observations Y_t are random variables that depend only on the state at that time t as well as on τ, where τ is the reporting rate.

The model was fitted to the data using particle filtering, which computes the probability of the data Y_t given the states X_t and is proportional to the likelihood function. At each day for a given spatial unit the binomial likelihood of the observed number of poliomyelitis cases was computed given the reporting rate τ and the simulated number of people completing the incubation period on that day. Therefore, the likelihood for a given district i was defined as:

$$L_{i,t} \sim \binom{H_{i,t}}{Y_{i,t}} \tau^{Y_{i,t}} (1-\tau)^{H_{i,t}-Y_{i,t}}$$

The likelihood across the period of observation and across all spatial units is therefore given as the product of conditional likelihoods across all observations and spatial units:

$$\prod_{t=1}^{T} \prod_{i=1}^{i=173} L_{i,t}$$

1.3 Initial conditions for parameter estimation

There were three sets of initial conditions for the model parameter estimation: 1) initialising the start of the model in 2010; 2) initialising the start of the modified model in April 2016 to account for changes due to OPV2 withdrawal; and 3) initialising the start of the Diamir outbreak in July 2019 (since the origin of this virus was not known and was not directly linked to any formal OPV2 use in Pakistan; therefore, it was not possible to directly generate the outbreak from the model).

Across all sets of initial conditions, the total number of children N_i in each district i was defined by extracting population data from WorldPop [22] and aggregating the total number at the district level. The population <3 years of age was determined by multiplying the total population by the proportion of the population <3 years of age in districts of Pakistan and Afghanistan (i.e. approx. 7% and 10% in Pakistan and Afghanistan, respectively)[23].

To initialise the start of the model in 2010, serotype-2 population immunity was estimated for Jan-Jun 2010 in Pakistan and Afghanistan and spatially and temporally smoothed, as in previously published methods [24, 25]. These estimates were used to infer the proportion of immune children R_i in each district i at the start of simulation. Given that the immunity estimates only capture vaccine-induced immunity, we increased the initial population immunity to account for secondary spread of OPV2 (i.e. Sabin virus) by multiplying the proportion susceptible by the amount of secondary spread (i.e. 42%) based on [7]. The number of exposed E_i and infected I_i children in each district i was initially set to zero and the number of susceptible S_i children was based on the remaining population <3 years (N_i) after accounting for R_i. All other compartments were set to zero. The starting conditions for April 2016 were consistent with those described for 2010 but with serotype-2 immunity based on estimates from Jan-Jun 2016 and the additional V_i compartment set to zero. The starting conditions of the outbreak in Diamir in July 2019 were determined through forward simulation from the modified model from April 2016. Based on re-initializing the model in July 2019, we then seeded cVDPV2 infection (i.e. 400 initial infections, corresponding to an expectation of 1 cVDPV2 case) in Diamir, Pakistan.

1.4 Parameter estimation

For 2010-2016, the parameters were estimated through maximizing the log likelihood of the model given the data using iterated particle filtering (mif2 function in the R package POMP [21]). The specifications for the iterated particle filtering algorithm were as follows: the variance factor was set to 1; the random walk standard deviation was set to 0.01; the number of particles was set to 1,000 per iteration; the number of iterations was set to 40 (20 iterations each with a cooling fraction, cf, of 0.5 and 0.2). The cooling fraction, cf, is the manner in which the intensity of the parameter perturbations is reduced with successive filtering iterations [21]. It is based on a geometric function,

defined by: $cf^{n/50}$, where n is the iteration number. The cooling factor allows the algorithm to jump from local maxima during the initial iterations. The inference algorithms in POMP require functions to be repeatedly evaluated, which can be quite computationally expensive. Therefore, the components of the transmission model were coded in the C programming language to speed up running time. These objects were dynamically linked into R and were called by the POMP object. To obtain profile log-likelihoods for each of the estimated parameters, the particle-filtering algorithm described above was run to maximize the log likelihood for 24 different fixed values, taken from a plausible range, for each of the three parameters. This process was repeated three times and an average of the maximized parameter estimates across the three runs was taken. The log likelihood was then evaluated five times for these final averaged parameter estimates, with each evaluated using 1,000 particles, and the mean maximized log likelihood was calculated. The log likelihood surface for each parameter was smoothed using the locally weighted scatterplot smoothing (loess) function in the R stats package [26].

For the calibration in 2019-2020, the parameters were estimated through maximizing the log likelihood of the model given the data using particle filtering across a reasonable range of parameter values identified in the iterated particular filtering for the 2010-2016 estimation. Moreover, the parameters were estimated across varying case to infection ratios (i.e. 1:400, 1:600, 1:800, 1:1000 and 1:2000) and amplitude A values. The log likelihood values of the best fit parameters were compared and those with the highest log likelihood were retained.

2 Results

2.1 Reported cVDPV2 cases

The first cVDPV2 case reported in the region was in Hilmand province, Afghanistan in June 2010 and was followed by 14 additional cases in Hilmand province and 4 in neighboring Kandahar province. The first cVDPV2 case in Pakistan was reported in the second half of 2012 in Killa Abdullah, Balochistan, and was followed by 86 additional cases concentrated in Balochistan, KP, KPTD and Karachi (last case reported prior to OPV2-withdrawal was in Feb 2015). In 2013-2014, North Waziristan reported a high of 49 cases.

2.2 Initial conditions

Population size <36 months of age was heterogeneous across Pakistan and Afghanistan (median 82,710, IQR [25,690-100,300]), with the greatest population in districts of Punjab (158,500, [99,090-223,300]) and the cities of Karachi (795,300) and Kabul (379,151). The lowest population size was in Balochistan (13,180, [7,692-22,540]).

In January-June 2010, the spatial distribution of serotype-2 population immunity was >80% in 87% of districts (median 92%, IQR [86%-95%]). The highest immunity was in Punjab (95%, [93%-

96%]) and the lowest immunity was in Balochistan (87%, [82%-92%]) and Southern Afghanistan (77%, [75%-82%]). Incorporating the impact of secondary spread of Sabin-2 vaccine virus, the population immunity to serotype-2 was ≥80% in 96% of districts (95%, [92%-97%]).

2.3 Vaccination

The number of SIA campaigns with tOPV in Pakistan and Afghanistan remained low and fairly consistent between January 2010 and June 2016 (Figure S4), with all districts (except North Waziristan) reporting at least 1 tOPV SIA per 1-year period. The number of mOPV2 and IPV SIAs between 1 July 2019 to 1 March 2020 remained focused primarily to Northern areas of Pakistan (i.e. Gilgit-Baltistan) and KP province (apart from 2 districts of Punjab); and are presented in Figure S5. IPV was conducted in Gilgit-Baltistan and Lahore.

Figure S4: Number of tOPV SIAs in Pakistan and Afghanistan in 6-month time periods between January 2010 and June 2016.

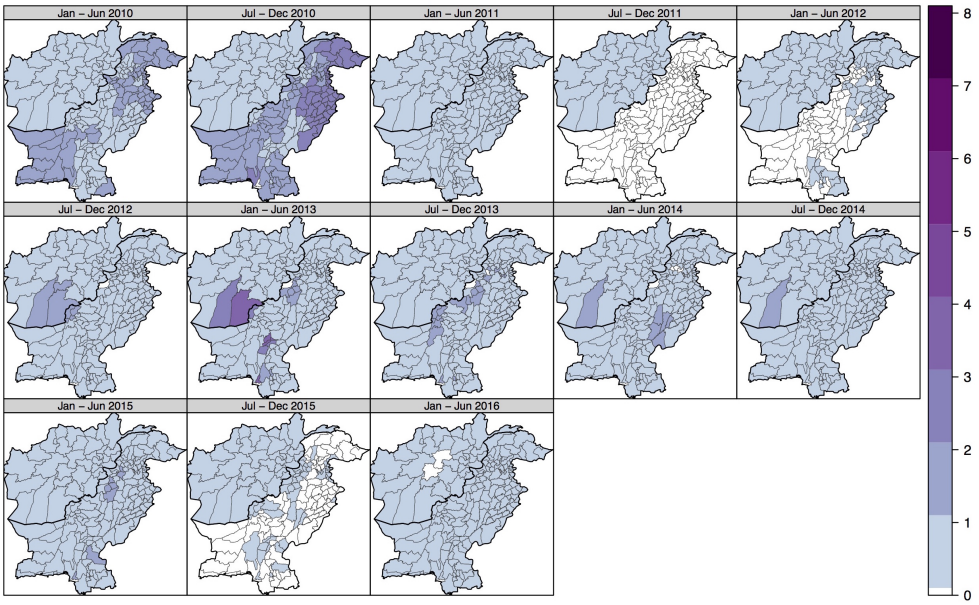

Figure S5: Number of mOPV2 and IPV SIAs between 1 July 2019 to 1 March 2020.

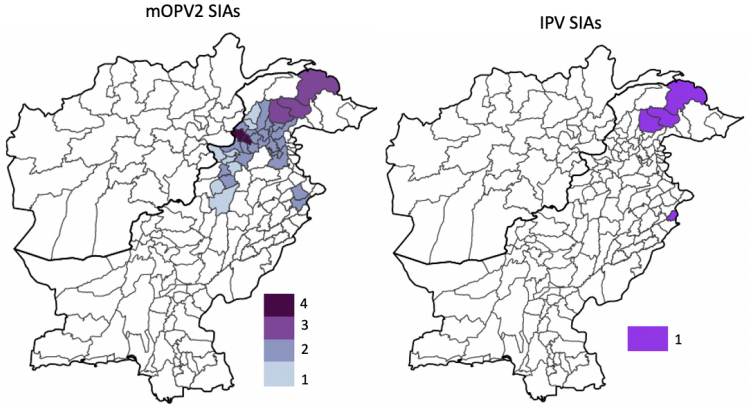

The estimated coverage of vaccination through RI and SIAs in 6-month time periods between January 2010 and June 2016 in Pakistan and Afghanistan are presented in Figure S6 and Figure S7, respectively.

Vaccination coverage of three doses of tOPV delivered through RI was spatially heterogeneous across Pakistan and Afghanistan (Figure S6). In Jan-Jun 2010, RI coverage in Pakistan and Afghanistan was 63% (IQR: 41-77%). In Pakistan, the highest RI coverage in was AJK (82%) and Punjab (78%); and the lowest was Balochistan (22%) and Sindh (51%). In Afghanistan, the highest RI coverage was Lagar (90%) and Nangarhar (82%); and lowest was Hilmand (15%) and Zabul (17%).

Figure S6: Estimates of cohort RI coverage (%) for children <36 months in Pakistan and Afghanistan (from 2010 to 2016).

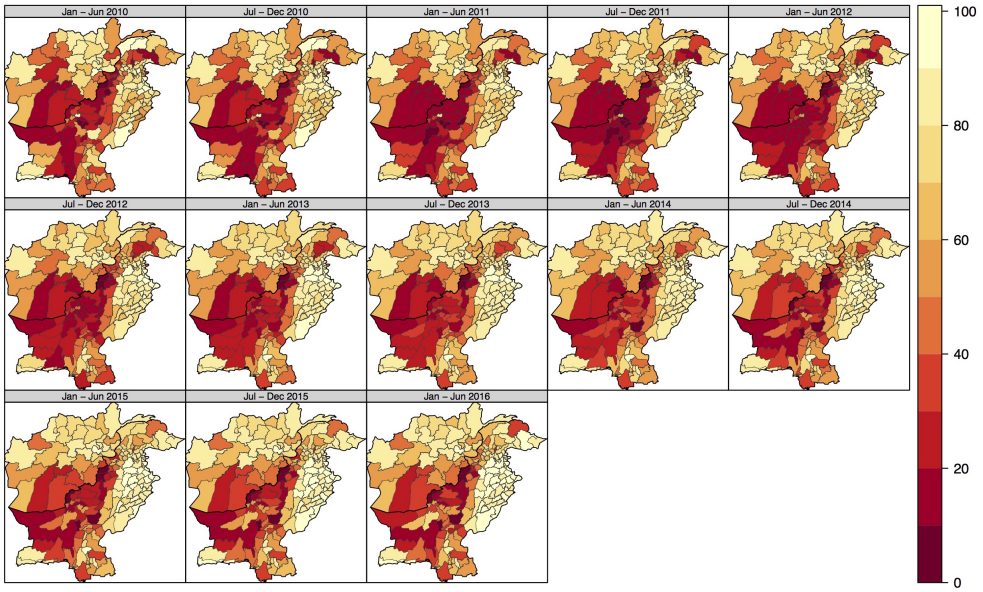

In Jan-Jun 2010, SIA coverage in Pakistan and Afghanistan was 69% (IQR: 57-80%) (Figure S7). In Pakistan, the highest SIA coverage in was Punjab (78%) and AJK (72%); and the lowest was Balochistan (56%) and Sindh (58%). In Afghanistan, the highest SIA coverage was Nangarhar (97%) and Laghman (96%); and lowest was Panjsher (52%) and Uruzgan (57%).

Figure S 7: Estimates of cohort SIA coverage (%) for children <36 months in Pakistan and Afghanistan (from 2010 to 2016).

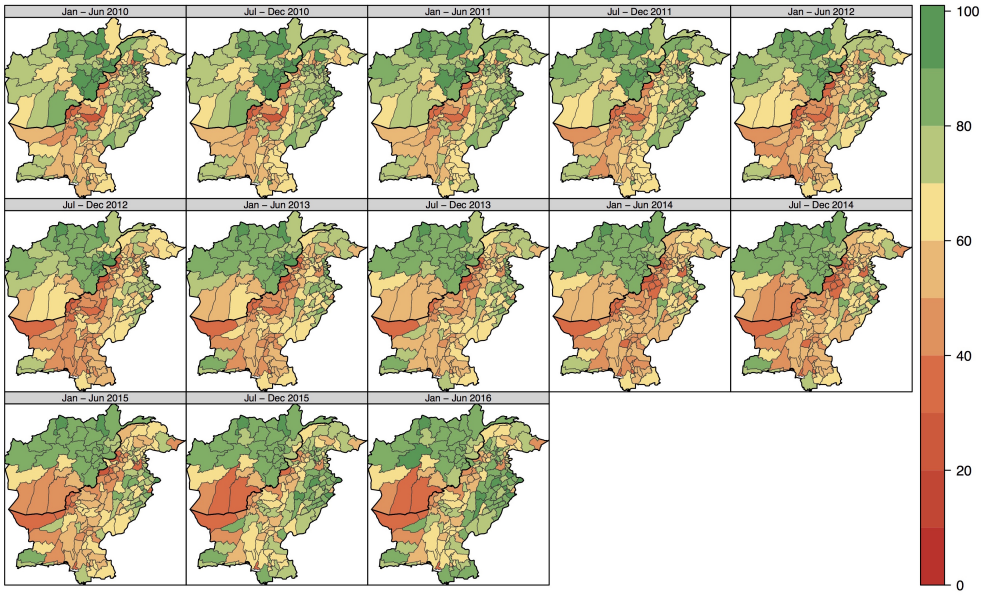

2.4 Parameter estimation

The log-likelihood profiles for the 2010-2016 estimated parameters are presented in Figure S8.

Figure S8: Log likelihood profiles for parameters estimated from the cVDPV2 transmission model. (A) Local transmission. (B) Local scaling factor for between-district transmission. (C) Reversion parameter.

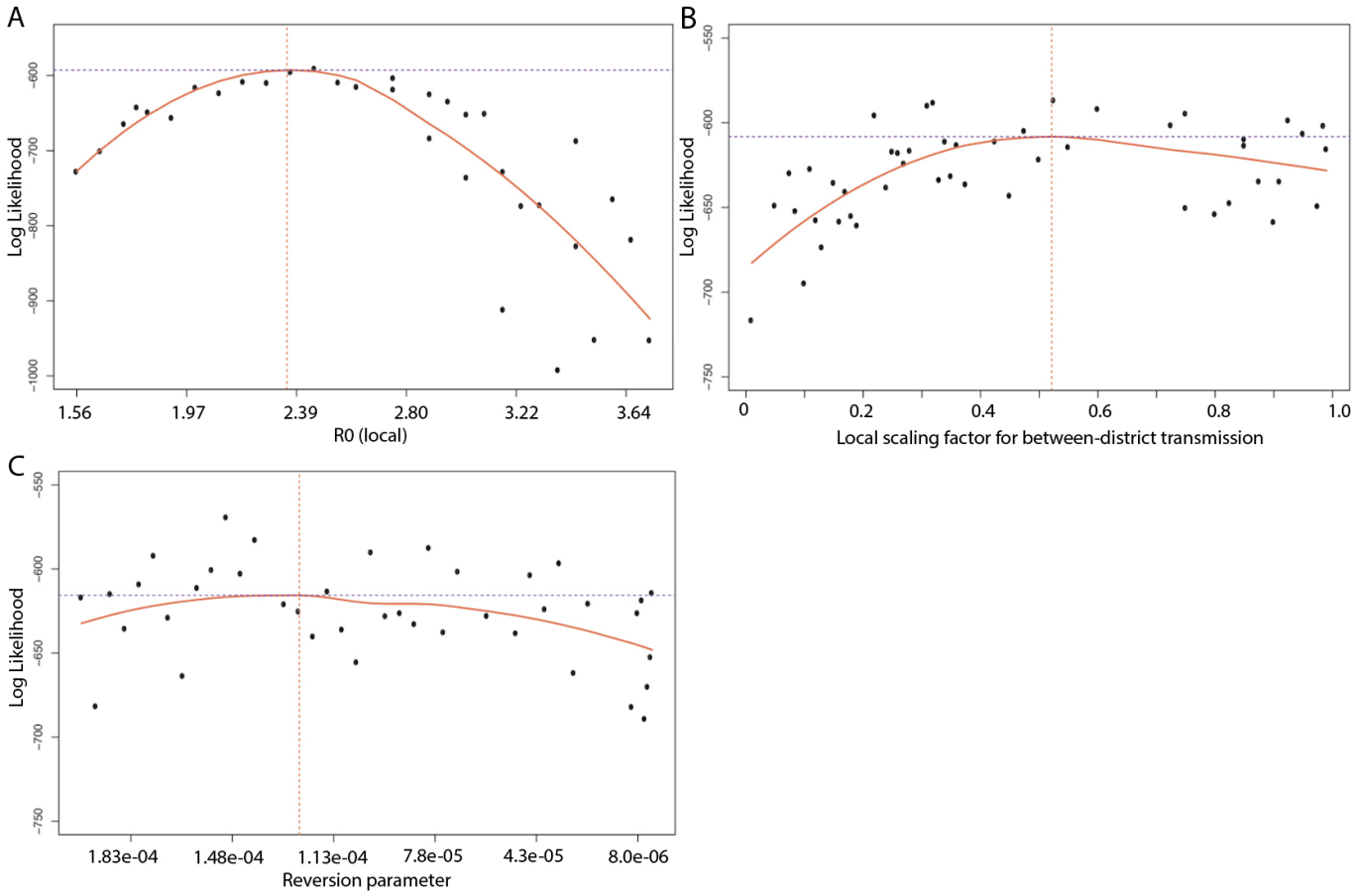

For the calibration to the Diamir outbreak between 2019-2020, the case to infection ratio of 1:400 resulted in a better log likelihood than lower values as did the amplitude scaled by a factor of 0.55 to account for the decrease in overall R_0 (i.e. A=11% based on scaling the A of 21% estimated from WPV1 transmission model by a factor of 0.55) (Table S3).

Table S3: Log likelihood values for case to infection ratios and amplitude

Case:infection	A=11%	A=21%
1:400	-375.0	-379.5
1:600	-379.3	-391.9
1:800	-380.6	-392.3
1:1000	-385.3	-394.6
1:2000	-385.4	-394.8

2.5 Impact of vaccination responses on 2019-20 cVDPV2 outbreak

Figure S9: Forward simulation of cVDPV2 outbreak originating in Diamir, Pakistan, considering impact of different vaccination strategies. Impact of number, timing and geographic scope (i.e. National and Sub-National) of SIAs based on assumption of (A) substantial reduction and (B) complete halt in transmission between Mar-Jun 2020.

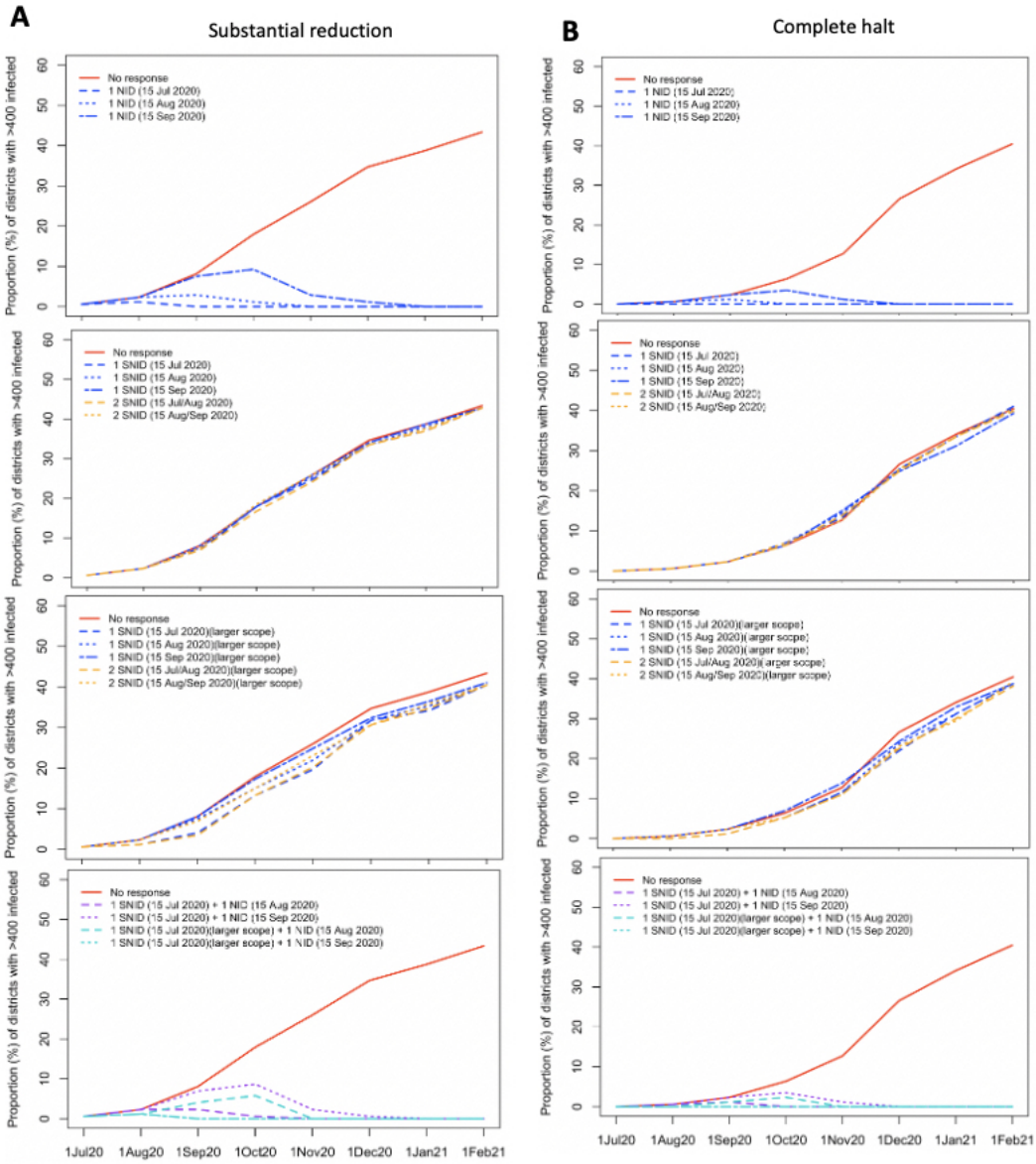

Figure S10: Forward simulation of cVDPV2 outbreak originating in Diamir, Pakistan, considering (A) substantial reduction and (B) complete halt in transmission between March-June 2020. Impact of proposed SIAs in proportion of districts with >400 cVDPV2 infections under estimated and reduced SIA coverage and considering responses with and without NIDs.

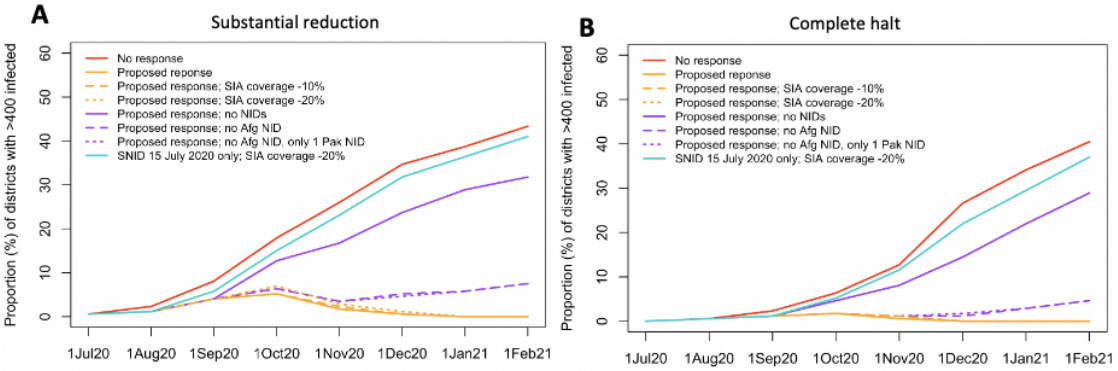

2.6 Risk of seeding cVDPV2 transmission due to mOPV2 response

Figure S11: Risk of emergence and spread of reverted Sabin2 from proposed SIA response (based on substantial reduction in transmission between March-June 2020). (A) Proportion of districts with any (i.e. >0) and >100 reverted Sabin2 infections over time under proposed response, reduced SIA coverage, and without NIDs. (B) Geographic distribution of number of reverted Sabin2 infections over time based on proposed response with and without NIDs.

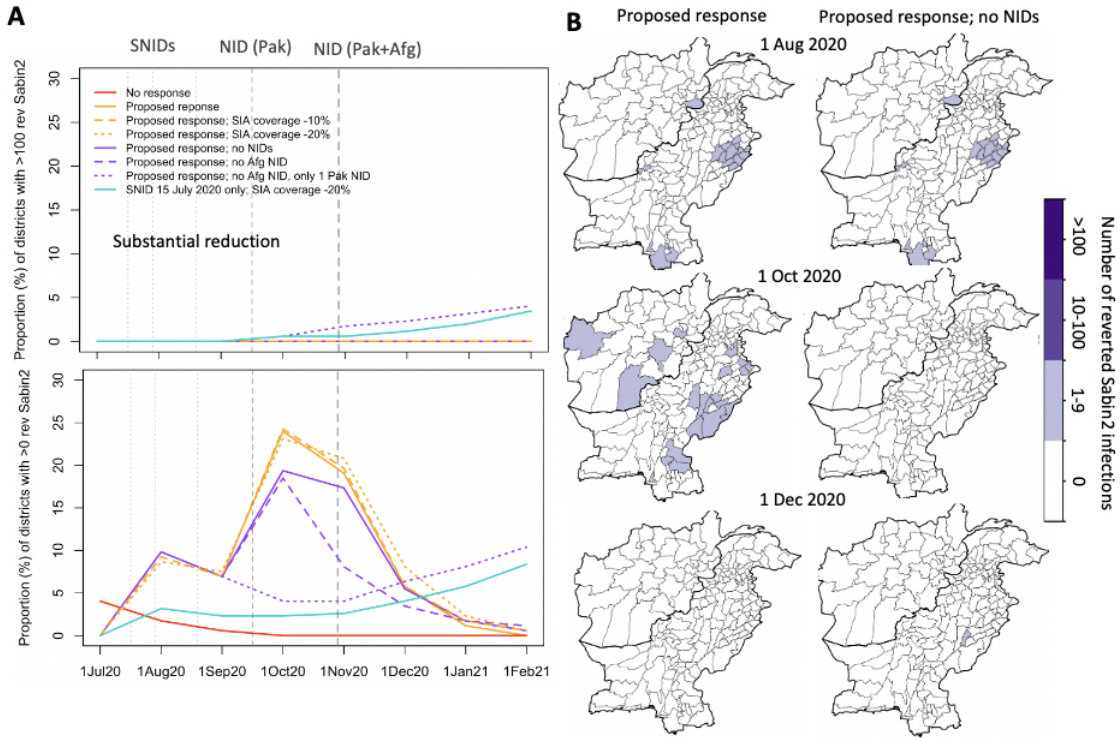

Figure S12: Risk of emergence and spread of reverted Sabin2 from proposed SIA response (based on complete halt in transmission between March-June 2020). (A) Proportion of districts with any (i.e. >0) and >100 reverted Sabin2 infections over time under proposed response, reduced SIA coverage, and without NIDs. (B) Geographic distribution of number of reverted Sabin2 infections over time based on proposed response with and without NIDs.

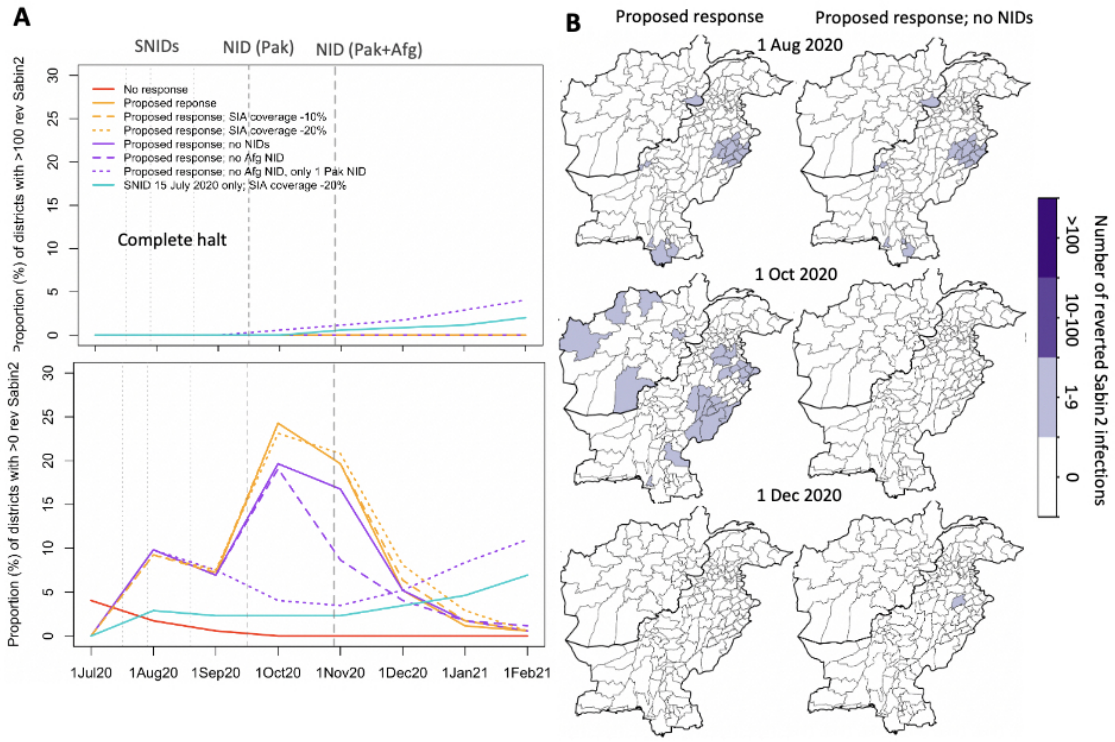

2.7 Sensitivity analysis with case-to-infection ratio 1:2000

The case to infection ratio for cVDPV2 is not conclusively determined and 1:400 may be an overestimate as some sources infer a lower ratio of up to 1:2000 ([17], [27]). While the lower ratio demonstrated little difference in the results within the first 1.5 years of the outbreak, predictions under the lower ratio resulted in a decline of the outbreak in late 2020, due to the increased spread of natural immunity in a shorter time frame, resulting in an overall lower predicted cumulative case burden by early 2021 (Figure S14,Figure S15). Despite this difference, the inferences from the proposed vaccination response remain the same.

Figure S13: Model validation. Monthly incidence of cVDPV2 observed cases (red line) and simulated cases (boxplots, across 100 simulations) in Pakistan and Afghanistan between 01 July 2019 to 29 February 2020, based on case-to-infection ratio of (A) 1:400; and (B) 1:2000.

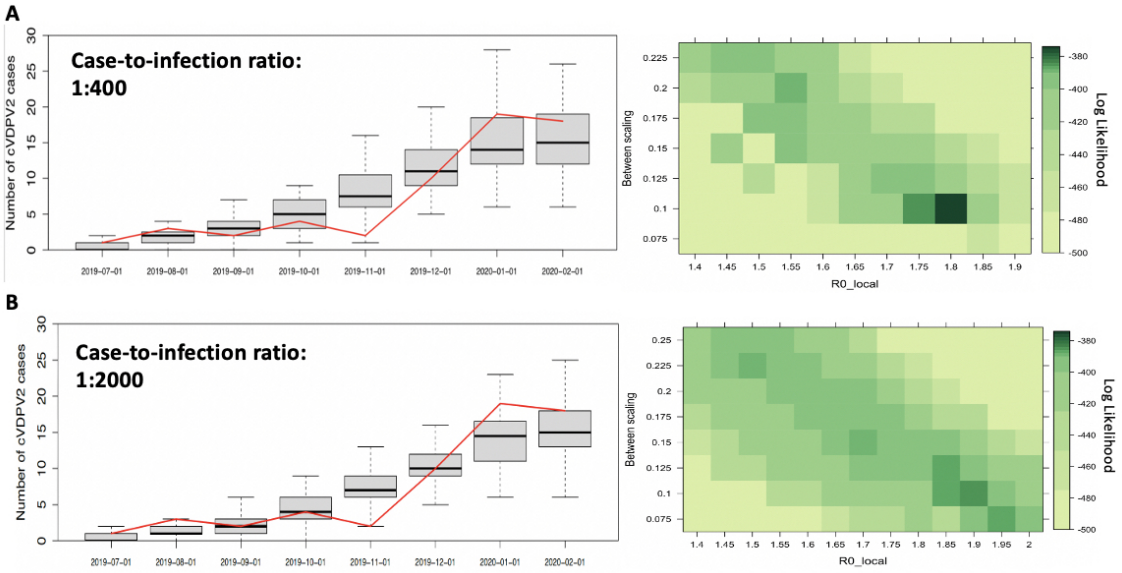

Figure S14: Forward simulation of cVDPV2 outbreak originating in Diamir, Pakistan, considering impact of proposed vaccination response, based on case-to-infection ratio of (A) 1:400; and (B) 1:2000.

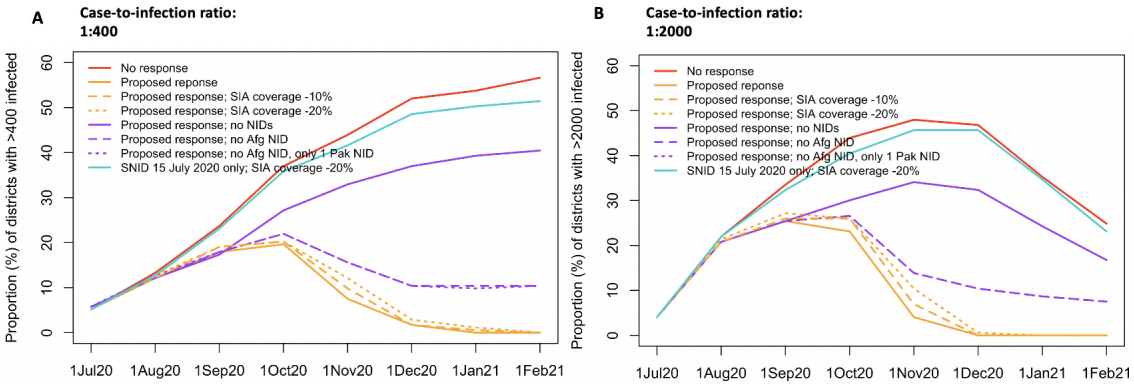

Figure S15: Distribution of cumulative number of cVDPV2 cases between July 2019 to November 2020 (top panel) and July 2019 to February 2021 (bottom panel) for the different assumptions of movement and vaccination strategies, based on case-to-infection ratio of (A) 1:400; and (B) 1:2000.

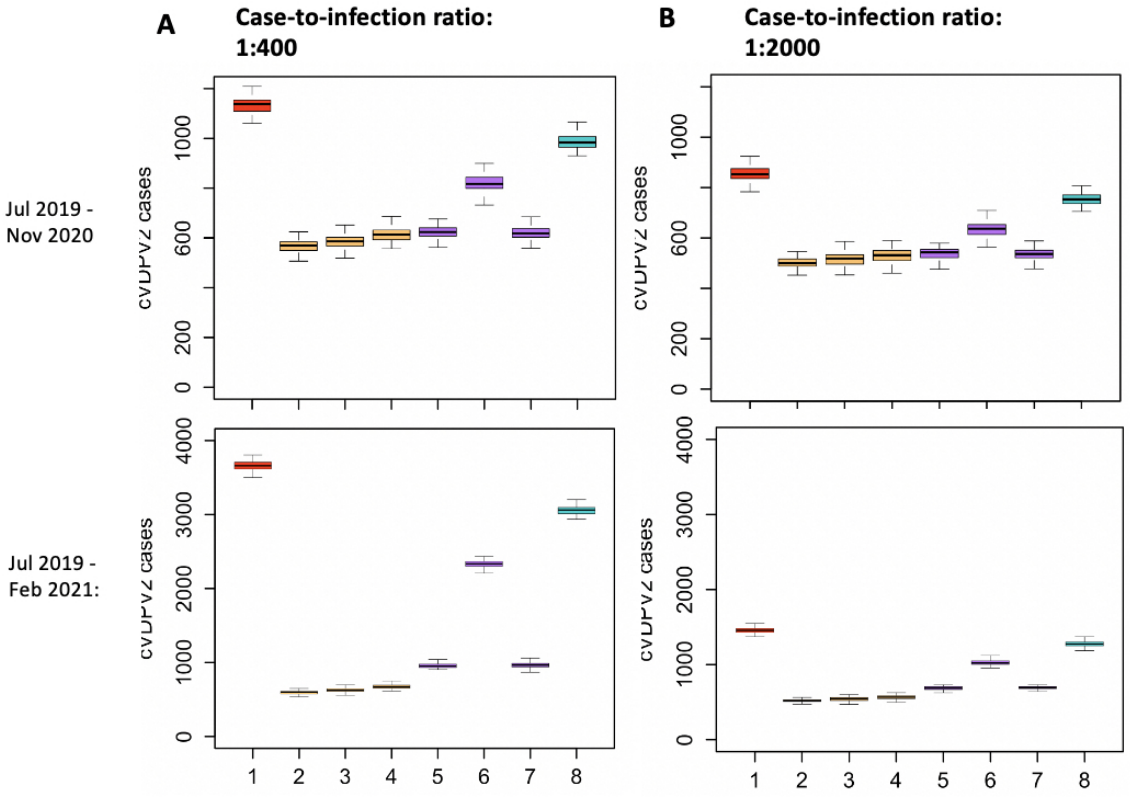

2.8 Actual OPV2 response between 1 July 2019 to 1 February 2021

Figure S16: Total and monthly number of OPV2 SIAs (i.e., mOPV2/tOPV)

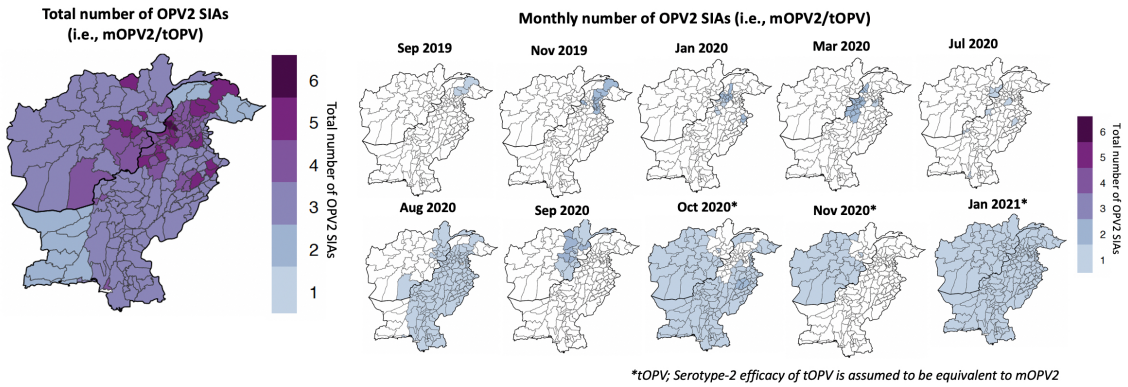

2.9 Exploring the impact in Pakistan of large-scale continued cVDPV2 transmission in Afghanistan

Exploring the impact in Pakistan of large-scale continued cVDPV2 transmission in Afghanistan (to reflect major access challenges and inability to conduct large-scale campaigns) through an extreme

scenario assuming no OPV2 SIAs in Afghanistan from 1 Oct 2020 (excluding 3 NIDs — Oct/Nov and Jan). This scenario also assumes reduced SIA coverage in Pakistan by 20%.

Despite the very high-levels of transmission in Afghanistan and the lower assumed coverage in Pakistan, the relatively high immunity in Pakistan is able to largely protect the population from large-scale cVDPV2 transmission. Based on this scenario, pockets of transmission persist in high-risk areas of Pakistan with low levels of coverage, with transmission increasing as type-2 mucosal immunity begins to wane.

Figure S17: Monthly simulated number of cVDPV2 infections

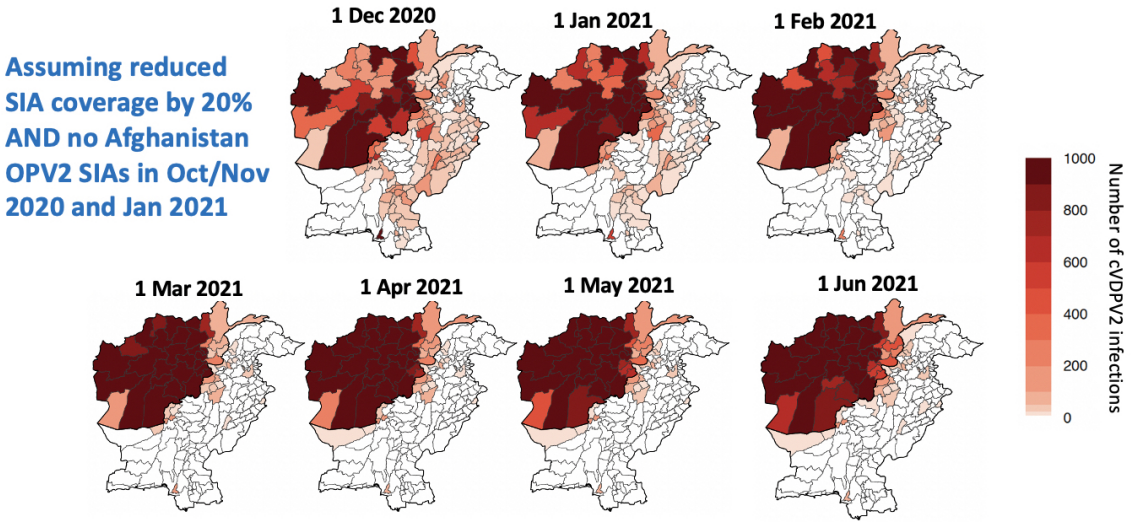

3 Supplementary Appendix I: WPV1 transmission model

In order to estimate the amplitude of seasonal forcing on poliovirus transmission, we developed a similar spatio-temporal stochastic mathematical model as described above but fitted it to historic daily incidence of WPV1 for 2010-2016. Parameters estimated include local and between district transmission coefficients, and the strength of seasonal forcing on transmission (i.e. Amplitude). The iterated particle filtering algorithm was repeated across different initial conditions to check convergence and precise estimates and log likelihood values.

3.1 Methods

The stochastic equations describing the state transitions of the transmission model are defined for each district i, as follows:

$$S_{i,t} = S_{i,t-1} - Z_t^{S_iE_i} - Z_t^{S_iD_i} + Z_t^{N_iS_i} - Z_t^{N_iR_i} - Z_t^{S_iR_i}$$
$$E_{i,t} = E_{i,t-1} + Z_t^{S_iE_i} - Z_t^{E_iI_i} - Z_t^{E_iD_i}$$
$$I_{i,t} = I_{i,t-1} + Z_t^{E_iI_i} - Z_t^{I_iR_i} - Z_t^{I_iD_i}$$
$$R_{i,t} = R_{i,t-1} + Z_t^{I_iR_i} - Z_t^{R_iD_i} + Z_t^{S_iR_i} + Z_t^{N_iR_i}$$

where the $Z_t^{S_iE_i}$, $Z_t^{E_iI_i}$ and $Z_t^{I_iR_i}$ correspond to the number of children moving from states S_i to E_i, E_i to I_i and I_i to R_i, respectively, at time t; $Z_t^{S_iD_i}$, $Z_t^{E_iD_i}$, $Z_t^{I_iD_i}$ and $Z_t^{R_iD_i}$ correspond to the number of children dying, D, in states S_i, E_i, I_i and R_i, respectively, at time t; and $Z_t^{N_iS_i}$ and $Z_t^{N_iR_i}$ correspond to the number of births entering state S_i and R_i, respectively, at time t, with N_i corresponding to the total population <36 months in district i at time t.

The number of children moving between states at time t is determined by drawing random numbers from the multinomial and binomial distributions based on the probability defined by the transition rates for each state already described for the cVDPV2 model. In the observation model for WPV1, we assumed a case to infection ratio of 1:200, as is commonly defined for serotype-1 poliomyelitis [17].

Using the model, we estimated three parameters: i) local transmission coefficient (i.e. β_l); ii) scaling factor for between-district transmission (i.e. $\beta_b = \beta_l f$, whereby f is the estimated parameter); and iii) the strength of seasonal forcing on transmission (i.e. amplitude A of transmission).

The parameters were estimated through maximizing the log likelihood of the model given the data using iterated particle filtering (mif2 function in the R package POMP [21]). The same specifications for the iterated particle filtering algorithm were used; however, the number of particles was set to 10,000 per iteration; the number of iterations was set to 40 (20 iterations each with a cooling fraction, cf, of 0.5 and 0.2). To obtain profile log-likelihoods for each of the estimated parameters, the particle-filtering algorithm described above was run to maximize the log likelihood for 24 different fixed values, taken from a plausible range, for each of the three parameters.

Table S4: Input parameter estimates for the WPV1 transmission model.

Parameters	Estimates (95% CIs)	Source
Recovery rate, γ	1/14	Evidence from[1][1]
Reporting rate, τ	1/200	Based on case to infection ratio [17]
Birth and death rate, μ	1/1581 per day	Based on median time in cohort (3 years)
Latency period, ν	4 days	Evidence from [4]
Secondary spread of OPV	42%	Seroprevalence in non-immunized populations [7][2]
Phase shift (peak) of amplitude, ϕ	July 16	Evidence from [17, 4] and preliminary genetic analysis [3]
Efficacy of tOPV (serotype-1)	0.125	Evidence from [28]
Efficacy of bOPV (serotype-1)	0.23	Evidence from [28]
Efficacy of mOPV1 (serotype-1)	0.23	Based on non-inferiority with bOPV [29]

[1] Duration of infectiousness based on this study was extended given the greater contribution of fecal-oral transmission in this population (which has longer shedding of virus compared to oral-oral transmission [16]). [2] Assuming same estimate of secondary spread used for serotype-2. [3] Preliminary genetic analysis of WPV1 sequences reported from Pakistan using methods described in [18].

3.2 Results

The model demonstrated good fit to the observed WPV1 cases and was able to reliably capture the spatio-temporal dynamics of WPV1 transmission in Afghanistan and Pakistan (Figure S18). In Pakistan, the model overestimated and underestimated the number of WPV1 cases in Jul-Dec 2013 and Jul-Dec 2014, respectively. The discrepancy in 2013 was likely due to issues with the SIA calendar data and in 2014 was due to geo-political factors resulting in sudden increases in movement dynamics. Moreover, the spatial distribution of overall WPV1 cases simulated from the model aligns with observed WPV1 cases (Figure S19).

Figure S18: Monthly incidence of WPV1 observed and simulated cases in Pakistan and Afghanistan in 6-month time periods between January 2016 to June 2016. Red line corresponds to monthly observed WPV1 cases. Boxplot correspond to distribution of WPV1 cases from 100 simulations of the model. (A) Pakistan and Afghanistan; (B) Pakistan; and (C) Afghanistan.

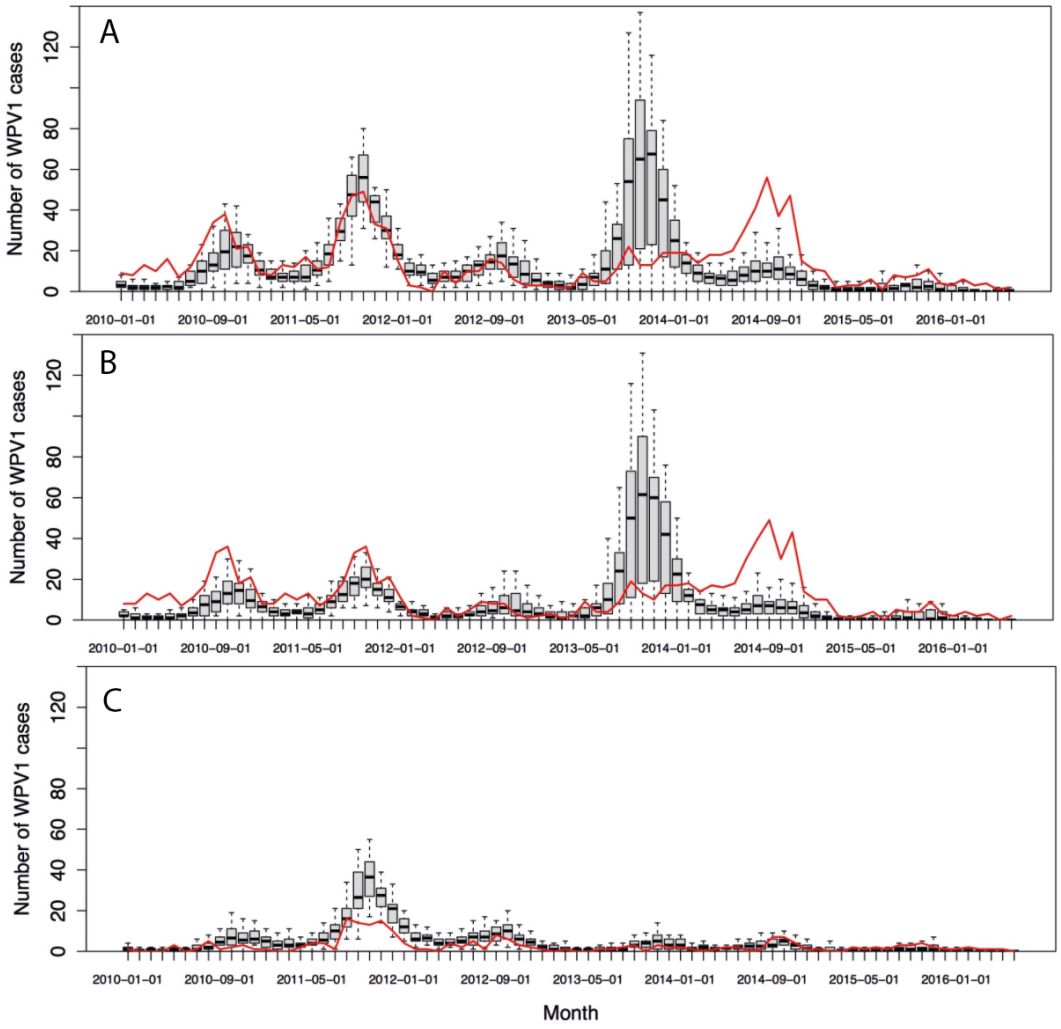

Figure S19: Spatial distribution of total number of WPV1 observed and simulated cases in Pakistan and Afghanistan between 2010-2016. (A) Observed WPV1 cases. (B) Simulated WPV1 cases (based on 1 simulation from the model). (C) Distribution of simulated WPV1 cases (i.e. lower quantile, median and upper quantile) (based on 100 simulations from the model).

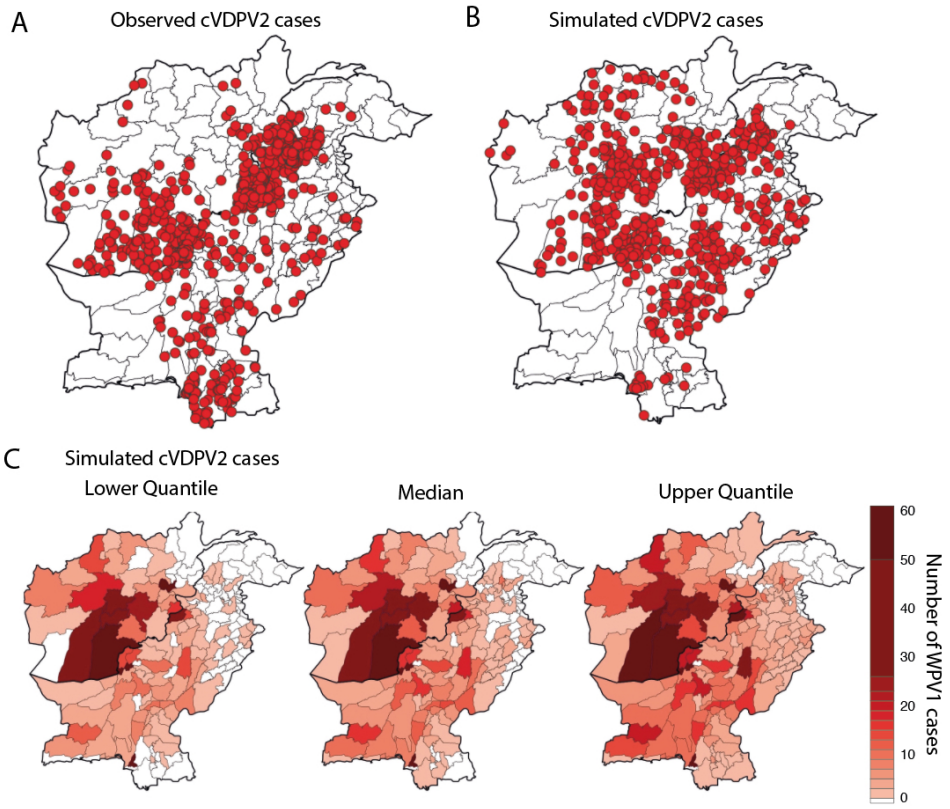

The local and overall R_0 were estimated to be 3.07 and 5.06, respectively. The local scaling factor for between-district transmission was 0.65 and the amplitude of the seasonal forcing was estimated to be 21%. The log-likelihood profiles for the estimated parameters are presented in (Figure S20A-C).

Figure S20: Log likelihood profiles and correlation for parameters estimated from WPV1 transmission model. (A) Amplitude of seasonal forcing on transmission. (B) Local transmission. (C) Local scaling factor for between-district transmission.

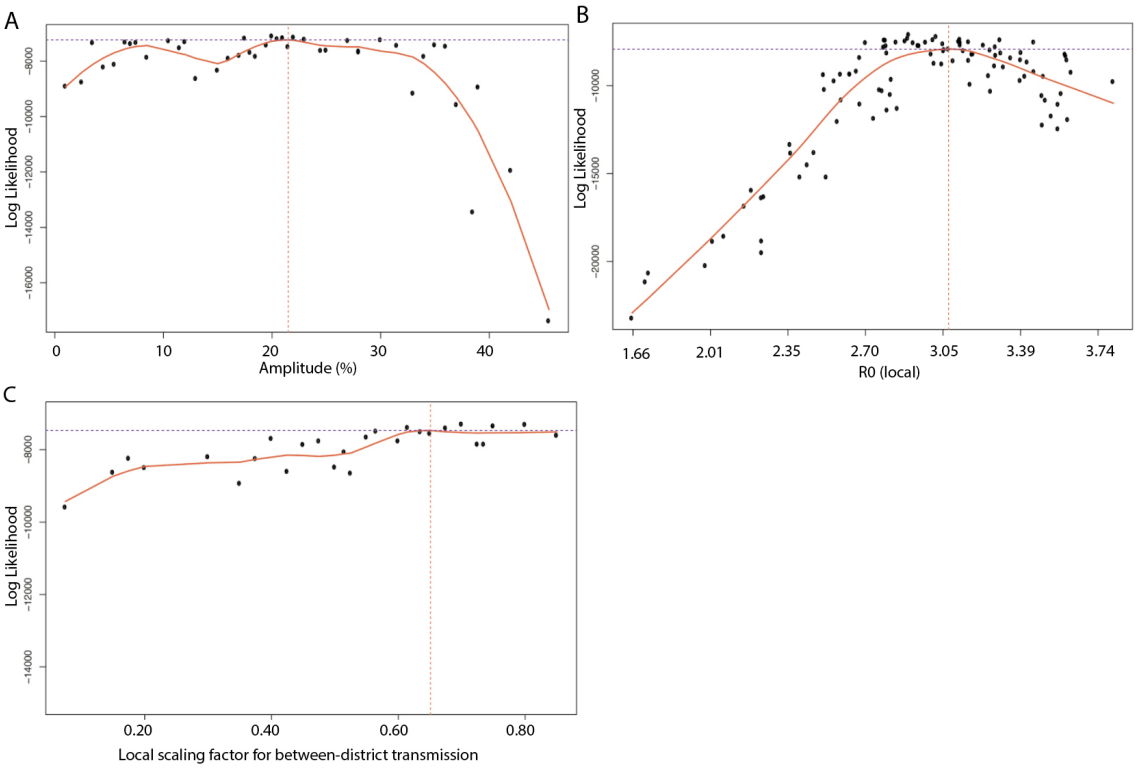

References

[1] Blake, I. M. *et al.* The role of older children and adults in wild poliovirus transmission. *Proceedings of the National Academy of Sciences* **111**, 10604–10609 (2014).

[2] Melnick, J. & Ledinko, N. Development of neutralizing antibodies against the three types of poliomyelitis virus during an epidemic period; the ratio of inapparent infection to clinical poliomyelitis. *Am J Hyg* **58**, 207–22 (1953).

[3] Gelfand, H., LeBlanc, D., Fox, J. & Conwell, D. Studies on the development of natural immunity to poliomyelitis in Louisiana II. Description and analysis of episodes of infection observed in study households. *Am J Hyg* **65**, 367–85 (1957).

[4] Grassly, N. C. *et al.* New strategies for the elimination of polio from India. *Science* **314**, 1150–1153 (2006).

[5] Blake IM, M. N. e. a., Pons-Salort M. Type 2 Poliovirus Detection after Global Withdrawal of Trivalent Oral Vaccine. *N Engl J Med* **379**, 834–845 (2018).

[6] SAGE meeting. Cessation Risk Assessment Meeting, June 13-14, 2017: Summary (October 2017). URL `http://www.who.int/immunization/sage/meetings/2017/october/presentations_background_docs/en/`.

[7] Chen, R. *et al.* Seroprevalence of antibody against poliovirus in inner-city preschool children. Implications for vaccination policy in the United States. *JAMA* **275**, 1639–45 (1996).

[8] Grassly, N. *et al.* Waning intestinal immunity after vaccination with oral poliovirus vaccines in India. *J Infect Dis* **205**, 1554–61 (2012).

[9] Mangal, T. *et al.* Key issues in the persistence of poliomyelitis in Nigeria: a case-control study. *Lancet Glob Health* **2** (2014).

[10] Patriarca, P., Wright, P. & John, T. Factors affecting the immunogenicity of oral poliovirus vaccine in developing countries: Review. *Reviews of Infectious Diseases* **13**, 926–39 (1991).

[11] Zaman K, M. M. e. a., Estívariz CF. Immunogenicity of type 2 monovalent oral and inactivated poliovirus vaccines for type 2 poliovirus outbreak response: an open-label, randomised controlled trial. *Lancet Infect Dis* **18**, 657–665 (2018).

[12] Asturias EJ, S. S. e. a., Bandyopadhyay AS. Humoral and intestinal immunity induced by new schedules of bivalent oral poliovirus vaccine and one or two doses of inactivated poliovirus vaccine in Latin American infants: an open-label randomised controlled trial. *Lancet* **388**, 158–169 (2016).

[13] Macklin GR, S. R. e. a., Grassly NC. Vaccine schedules and the effect on humoral and intestinal immunity against poliovirus: a systematic review and network meta-analysis. *Lancet Infect Dis* **19**, 1121–1128 (2019).

[14] WHO. Immunogenicity of mOPV2 administered as 1-drop or 2-drops: summary of preliminary results (2019). URL `Available:https://www.who.int/immunization/sage/meetings/2019/october/3_Preliminary_Results_mOPV2_one_drop_trial_v_2.pdf?ua=1`.

[15] Grassly, N. C. Immunogenicity and Effectiveness of Routine Immunization With 1 or 2 Doses of Inactivated Poliovirus Vaccine: Systematic Review and Meta-analysis. *Journal of Infectious Diseases* **210**, S439–S446 (2014).

[16] Garon, J., Cochi, S. & Orenstein, W. The challenge of global poliomyelitis eradication. *Infect Dis Clin N Am* **29**, 651–665 (2015).

[17] Nathanson, N. & Kew, O. From emergence to eradication: the epidemiology of poliomyelitis deconstructed. *Am J Epidemiol* **172**, 1213–29 (2010).

[18] Li, L., Grassly, N. & C, F. Quantifying Transmission Heterogeneity Using Both Pathogen Phylogenies and Incidence Time Series. *Molecular Biology and Evolution* **34**, 2982–2995 (2017).

[19] Casey, A. E. Observations on an Epidemic of Poliomyelitis. *Science* **95**, 359–360 (1942).

[20] Casey, A. E. The incubation period in epidemic poliomyelitis. *JAMA* **120**, 805–807 (1942).

[21] King, A., Nguyen, D. & Ionides, E. Statistical Inference for Partially Observed Markov Processes via the R Package pomp. *Journal of Statistical Software* **69**, 1–43 (2016).

[22] WorldPop Project. URL `www.worldpop.org.uk`.

[23] United States Census Bureau. International Programs. Available at: https://www.census.gov/data-tools/demo/idb/informationGateway.php .

[24] Pons-Salort, M. *et al.* Population immunity against serotype-2 poliomyelitis leading up to the global withdrawal of the oral poliovirus vaccine: Spatio-temporal modelling of surveillance data. *PLoS Medicine* **13** (2016).

[25] Molodecky, N. *et al.* Risk factors and short-term projections for serotype-1 poliomyelitis incidence in Pakistan: A spatiotemporal analysis. *PLoS Medicine* **14** (2017).

[26] R Core Team. *R: A Language and Environment for Statistical Computing*. R Foundation for Statistical Computing, Vienna, Austria (2015). URL `https://www.R-project.org/`.

[27] Wringe, A., Fine, P., Sutter, R. & Kew, O. Estimating the extent of vaccine-derived poliovirus infection. *PLOS One* **3**, e3433 (2008).

[28] O'Reilly, K. M. *et al.* The effect of mass immunisation campaigns and new oral poliovirus vaccines on the incidence of poliomyelitis in Pakistan and Afghanistan, 2001–11: a retrospective analysis. *Lancet* **380**, 491–498 (2012).

[29] Sutter, R. *et al.* Immunogenicity of bivalent types 1 and 3 oral poliovirus vaccine: a randomised, double-blind, controlled trial. *Lancet* **376**, 1682–88 (2010).